

# PVT: Point-Voxel Transformer for Point Cloud Learning

Zhang Cheng<sup>1\*</sup>, Haocheng Wan<sup>1\*</sup>, Xinyi Shen<sup>2</sup>, Zizhao Wu<sup>1†</sup>

<sup>1</sup>Hangzhou Dianzi University, Hangzhou China

<sup>2</sup>University College London, London UK

{zhangcheng828, wanhaocheng2022, xinyishen2018, wuzizhao}@foxmail.com, @163.com, @hdu.edu.cn

## Abstract

The recently developed pure Transformer architectures have attained promising accuracy on point cloud learning benchmarks compared to convolutional neural networks. However, existing point cloud Transformers are computationally expensive since they waste a significant amount of time on structuring the irregular data. To solve this shortcoming, we present Sparse Window Attention (SWA) module to gather coarse-grained local features from non-empty voxels, which not only bypasses the expensive irregular data structuring and invalid empty voxel computation, but also obtains linear computational complexity with respect to voxel resolution. Meanwhile, to gather fine-grained features about the global shape, we introduce relative attention (RA) module, a more robust self-attention variant for rigid transformations of objects. Equipped with the SWA and RA, we construct our neural architecture called PVT that integrates both modules into a joint framework for point cloud learning. Compared with previous Transformer-based and attention-based models, our method attains top accuracy of 94.0% on classification benchmark and 10× inference speedup on average. Extensive experiments also valid the effectiveness of PVT on part and semantic segmentation benchmarks (86.6% and 69.2% mIoU, respectively).

**Keywords** Point Cloud Learning, Transformer, Neural Network, 3D Vision.

## 1. Introduction

Point cloud learning has been receiving increasing attention from both industry and academia due to its wide applications including autonomous driving, robotics, AR/VR, etc. In these settings, sensors like LIDAR produce irregular and unordered sets of points that correspond to object surfaces. However, how to capture semantics directly and quickly from this data remains a challenge for point cloud

learning.

Most existing point cloud learning methods could be classified into two categories in terms of data representations: the *voxel*-based models and the *point*-based models. The *voxel*-based models generally rasterize point clouds onto regular grids and apply 3D convolution for feature learning [61, 28, 43]. These models are computationally efficient due to their excellent memory locality, but the inevitable information loss degrades the fine-grained localization accuracy [33]. In contrast, the *point*-based models naturally preserve the accuracy of point location, but are generally computationally intensive [38, 3, 16].

Recently, Transformer has drawn great attention in natural language processing and 2D vision because of its superior capability in capturing long-range dependencies. Powered by Transformer [37] and its variants [24, 7], the *point*-based models have applied self-attention (the core unit of Transformer) to extract features from point clouds and improve performance significantly [12, 8, 59, 49]. However, most of them suffer from the time-consuming process of sampling and aggregating features from irregular points, which becomes the efficiency bottleneck [25].

In this paper, we study how to design an efficient and high-performance Transformer architecture while avoiding the shortcoming of previous point cloud Transformers. We observe that the *voxel*-based models have regular data locality and can efficiently encode coarse-grained features, while the *point*-based networks preserve the accuracy of location information with the flexible fields and can effectively aggregate fine-grained features. Inspired by this, we propose a novel point cloud learning architecture, named PVT that combines the ideas of *voxel*-based and *point*-based models. Our network focuses on how to fully exploit the potential of the two models mentioned above in Transformer architecture, capturing useful discriminative features from 3D data.

To investigate this, we conduct self-attention (SA) computation in *voxels* to obtain efficient learning pattern while performing SA in *points* to preserve the accuracy of location information with the flexible fields. However, directly performing SA computation to voxels is infeasible, mainly

\*These authors contributed equally.

†Corresponding author.

owing to two facts: Firstly, non-empty voxels are sparsely distributed in the *voxel* domain and only account for a small proportion of total voxels [50]. Secondly, the original SA computation leads to quadratic complexity with respect to the number of voxel grids, making it unsuitable for various 3D vision tasks, particularly for the dense prediction tasks of object detection and semantic segmentation. To tackle these issues, we design Sparse Window Attention (SWA) which only has linear computational complexity by computing SA locally within the non-overlapping 3D window. A key design element of SWA lies in its sparse attention computing, in which a GPU-based Rule Book stores the non-empty voxel indexes. Based on this strategy, we can bypass the invalid computation of empty voxels and retain the original 3D shape structure. For cross-window information interaction, inspired by Swin Transformer [24], we propose to apply shifted window to enlarge the receptive field. In addition, to enhance the global information awareness of SA computing in *points*, we propose relative-attention (RA) which extends the SA mechanism to consider representations of the relative position, or distances between points. Its advantage is that the absolute coordinates of the same object can be completely different with rigid transformations; thus, injecting relative position representations (RPR) in our structure is generally more robust. We observe that our network obtains significant improvements over not using this RPR term without adding extra training parameters.

Based on SWA and RA, We propose a two-branch PVT which mainly consists of the *voxel* branch and the *point* branch (see Figure 1). As illustrated in Figure 4, by behaving SWA in the *voxel* branch and performing RA in the *point* branch, our method disentangles the coarse-grained local feature aggregation and the fine-grained global context transformation so that each branch can be implemented efficiently and accurately.

By using the PVT, we construct Point-Voxel Transformer networks for various 3D tasks. These networks can capably serve as a general-purpose backbone for point cloud learning. In particular, we conduct the classification experiment on the ModelNet40 [44] dataset and obtain the state-of-the-art accuracy of 94.0% (no voting), while being on average  $10\times$  faster than its Transformer baselines. On ShapeNet Part [22] and S3DIS datasets [1], our model also obtains strong performance (86.6% and 69.2% mIoU, respectively).

The main contributions are summarized as following:

- We propose PVT, which is the first Transformer-based approach for deeply incorporating the advantages from both *point*-based and *voxel*-based networks to our knowledge.
- We propose an efficient local attention module, named SWA, which achieves linear computational complexity with respect to the input voxel size.

- We present RA module, a self-attention variant by considering the pairwise relationships or distance between input points.
- Extensive experiments show that our PVT model attains competitive results on general point cloud learning tasks with  $10\times$  latency speed-up than its baselines.

## 2. Related works

### 2.1. Voxel-based models on points

To leverage the success of convolutional neural networks on 2D images, many researchers have endeavored to project 3D point clouds directly onto voxels and perform 3D convolution for information aggregating [5, 19]. However, the memory and computational consumption of such full-voxel-based models increases cubically with respect to the voxel’s resolution. To tackle this shortcoming, O-CNN [40], OctNet [31] and kd-Net [15] constructed tree structures for 3D voxels to bypass the invalid computation of the empty voxels. Although such methods are efficient in data structuring, geometric details will be lost during the projection because multiple bucketing points into the same voxel leads to indistinguishable of features for learning.

Compared with most *voxel*-based 3D models, our model is more efficient and effective: 1) instead of using 3D convolutions, we propose SWA to handle the sparsity characteristic of voxels which has linear computational complexity with respect to voxel resolution and bypasses the invalid computation of empty voxels. 2) as we employ RA in the *point* domain, an inherent advantage is that we can avoid feature loss during voxelization, maintaining the geometric details of a point cloud.

### 2.2. Point-based models for point cloud learning

Instead of voxelization, it is possible to make a neutral network that consumes directly on point clouds. [27] proposed PointNet, the pioneering work that learns directly on sparse and unstructured point clouds. Inspired by PointNet, previous works introduced sophisticated neural modules to learn per-point features. These models can be generally classified as: 1) neighbouring feature pooling [57, 14], 2) graph message passing [42, 53, 39], and 3) attention-based or Transformer-based models [32, 54, 51, 12, 59, 8].

Due to the sparsity and irregularity of point clouds, the methods that directly consume points have achieved state-of-the-art performance. However, the cost of data structuring of such methods has become the computation burden especially on the large-scale point clouds dataset [25, 47]. In this paper, we handle this shortcoming by using the SWA module.

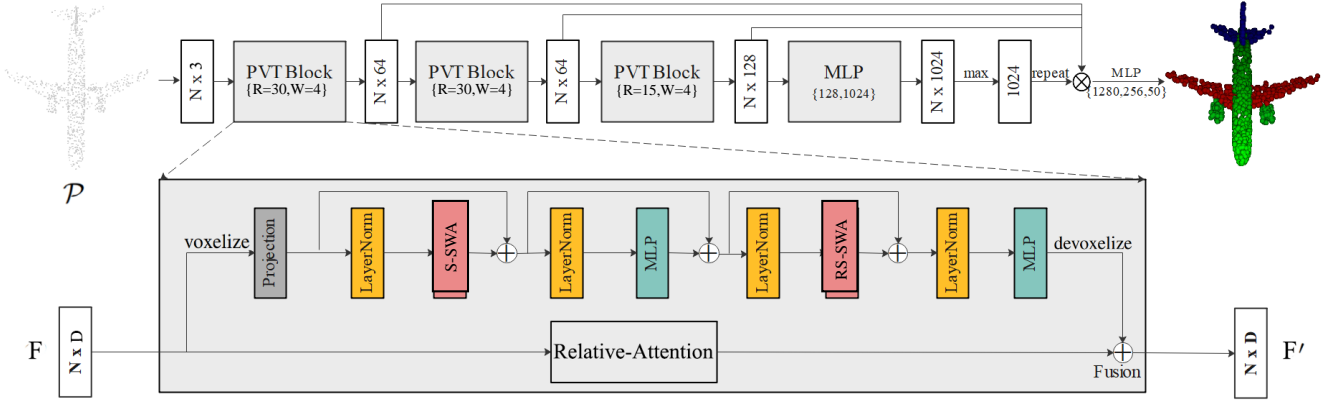


Figure 1. **Model Architecture:** The model for part segmentation take as input  $N$  points and feeds them into 3 stacked PVT blocks to learn a semantically rich and discriminative representation for each point, followed by a MLP layer to generate the output feature. After that, we leverage the max-pooling and repeating operators to extract an effective global feature representing the entire point cloud. Note that shortcut connections are used to extract multi-scale features and one MLP layer (1280) to aggregate multi-scale features, where we concatenate features from previous layers to get a  $64+64+128+1024=1280$ -dimensional point cloud. Finally, we predict the final point-wise segmentation scores for the input point cloud and the part label of a point is also determined as the one with maximal score. **PVT block (grey box):** The PVT block is composed of two branches. The upper branch is *voxel*-based for aggregating local features and the lower is *point*-based for capturing global features. We can effectively fuse two branches because they are providing complementary information.  $R$  and  $w$  denote the voxel resolution size and 3d window size, respectively.  $\oplus$ : addition,  $\otimes$ : concatenation.

### 2.3. Self-attention and Transformer

[2] proposed a neural machine translation method with an attention mechanism, in which attention weight is computed through the hidden state of an RNN. Then [23] further proposed self-attention to visualize and interpret sentence embeddings. Subsequent works employed self-attention layers to replace some or all the spatial convolution layers such as Transformer for machine translation [37]. [6] proposed bidirectional transformers (BERT), which is one of the most powerful models in the NLP field.

Witness the success of self-attention and Transformer architectures in NLP, researchers applied them to vision tasks [13, 30, 56]. For instance, [7] proposed an image recognition network, ViT, which directly applied a Transformer architecture on image patches and achieved better performance than the traditional convolutional neural networks. [24] recently introduced Swin Transformer to incorporate inductive bias for spatial locality, as well as for hierarchy and translation invariance.

Recently, plenty of researchers attempt to explore Transformer-based architectures for point cloud learning. Nico et al. [8] proposed  $PT^1$  to extract global features by introducing the standard SA mechanism. Guo et al. [12] proposed offset-attention to calculate the offset difference between the SA features and the input features by element-wise subtraction. And Zhao et al. [17] proposed  $PT^2$  to build local vector attention in neighborhood point sets and achieved significant progress. However, they wastes a high percentage of the total time on structuring the irregular data, which becomes the efficiency bottleneck. In this work, we

study how to solve this shortcoming, so as to design an efficient Transformer-based architecture for point cloud analysis.

## 3. Method

### Overview

In contrast to the previous point cloud Transformers [12, 8, 59], we design the network as efficient as possible with high accuracy so that it can be widely used on various 3D tasks.

We introduce an efficient neural architecture for point cloud learning: Point-Voxel Transformer (PVT). Formally, given a point cloud embedding  $F \in \mathbb{R}^{N \times D}$ , our PVT is designed to map the input features  $F$  to a new set of point feature  $F' \in \mathbb{R}^{N \times D}$ . As illustrated in Figure 1, the PVT consists of two main branches: a *voxel* branch and a *point* branch. We leverage the *voxel* branch to map the inputs  $F$  to  $F_{local} \in \mathbb{R}^{N \times D}$  which aggregates local features in the *voxel* domain. However, full *voxel* method will inevitably encounter information loss during voxelization. Thus, we utilize the *point* branch to map the inputs  $F$  to  $F_{global} \in \mathbb{R}^{N \times D}$ , which can directly extract global features for each individual point. With both local features and aggregated global context, we can efficiently fuse two branches into an addition layer as both provide complementary information.

Below we detail the two branches in Section 3.1 and 3.2 respectively. Section 3.3 details our feature fusion module. Finally, Section 3.4 discusses the relationship between the proposed model and the prior works.

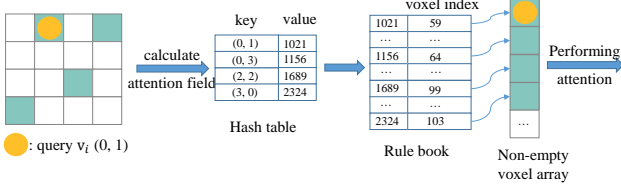


Figure 2. **Sparse Window Attention:** This is also a 2D example and can be easily extended to 3D cases. SWA is a GPU-based method and can efficiently index the non-empty voxels in the attention field.

### 3.1. The Voxel Branch

This branch aims to effectively capture local information, which can bypass expensive sampling and neighbor points querying. Specifically, it contains three steps: voxelization, feature aggregation and devoxelization.

The voxelized and devoxelized methods map the input point cloud  $\mathcal{P}$  to a new set of voxel features  $V$  and transform the voxel-wise features back to the point-wise features  $F_{local}$  (Readers can refer to [25] for more details). In this work, we apply the standard Transformer architecture [37] to perform feature aggregation on regular 3D voxel grids, which can improve accuracy significantly. However, the standard Transformer architecture conduct global-SA which leads to quadratic complexity with respect to the number of voxels, making it unsuitable for many 3D vision problems requiring dense prediction such as semantic segmentation.

**Window Attention:** To obtain efficient modeling power, we propose to compute SA within local 3D windows, which are arranged to evenly partition the voxel space in a non-overlapping manner. Assume that each local 3D window contains  $W \times W \times W$  voxel grids and  $R$  denotes the voxel resolution, the computational complexity of a global-SA and a window-based one on  $R^3$  voxel grids are:

$$\begin{aligned} \Omega(\text{Global-SA}) &= 4R^3D^2 + 2(R^3)^2D & (1) \\ \Omega(\text{Window-SA}) &= 4R^3D^2 + 2B^3R^3D & (2) \end{aligned}$$

where the former is quadratic to voxel grids number  $R^3$ , and the latter is linear when  $W$  is fixed,  $D$  is the dimension of features. In summary, global-SA computation is generally unaffordable for a large voxel resolution, while the local window-SA is scalable.

**Sparse Window Attention:** Different from 2D pixels which are densely placed on an image plane, non-empty voxels only account for a small proportion of total voxels. Inspired by [11, 50], we design Sparse Window Attention (SWA) to handle the sparsity characteristic of voxels. As shown in Figure 2, for each querying index  $v_i$ , we first use Window Attention to determine all neighboring voxel indexes in the attention field, and then adopt a Hash table to get the hashed integer neighboring voxel indices. Later, a

GPU-based Rule Book stores the hashed these voxel indices as keys, and the corresponding indices for the non-empty voxel array as values. Finally, we can perform Window Attention to gather the coarse-grained local features. Note that all the steps can be conducted in parallel on GPUs by assigning each querying voxel  $v_i$  a separate CUDA thread.

The SWA lacks information interaction across windows, which may limit the representation power of our model. Thus, we extend the shifted 2D window mechanism of Swin Transformer [24] to 3D windows for the purpose of introducing cross-window information interaction while maintaining the efficient computation of non-overlapping SWA. Readers can refer to Swin Transformer for more details

As shown in Figure 1, with the cyclic shifted window partitioning approach, the step of feature aggregation of this branch can be described as:

$$V^\ell = S\text{-SWA}(LN(V^{\ell-1})) + V^{\ell-1} \quad (3)$$

$$\hat{V}^\ell = MLP(LN(V^\ell)) + V^\ell \quad (4)$$

$$V^{\ell+1} = RS\text{-SWA}(LN(\hat{V}^\ell)) + \hat{V}^\ell \quad (5)$$

$$\hat{V}^{\ell+1} = MLP(LN(V^{\ell+1})) \quad (6)$$

where  $V^\ell$  and  $\hat{V}^\ell$  denote the output features of the S-SWA module and the MLP module for layer  $\ell$ , respectively; S-SWA and RS-SWA denote SWA computation using shifted and reverse shifted window partitioning configurations, respectively.

### 3.2. The Point Branch

The *voxel* branch gathers the neighborhood information with low-resolution. However, in order to capture long-range dependencies, low-resolution *voxel* branch alone is limited. To this end, we attempt to employ the standard self-attention on the entire point cloud for global context aggregation, which is computed as:

$$F_{sa} = \text{softmax}(QK^T)V, \quad F_{sa} \in \mathbb{R}^{N \times D} \quad (7)$$

$$F_{global} = MLP(F_{sa}) + F, \quad F_{global} \in \mathbb{R}^{N \times D} \quad (8)$$

where  $(Q, K, V) \in \mathbb{R}^{N \times D}$  is generated by shared linear transformations and the input features  $F$ , they are all ordered independent. Moreover, *softmax* and *weighted sum* are both permutation-independent operators. Thus, the standard self-attention computation is permutation-invariant, making it well-suited to handle the irregular, disordered 3D points.

However, the standard self-attention fails to incorporate relative position representations in its structure, while such ability is very important to 3D visual tasks. For example, the absolute coordinates of the same object can be completely different with rigid transformations. Therefore, injecting relative position representations are generally more

	Layer Type	Time Complexity per Layer
Voxel-based	3D Convolutions	$\mathcal{O}(k \cdot R^3 \cdot D^2)$
	SWA	$\mathcal{O}(v \cdot R^3 \cdot D)$
Point-based	1D Convolutions	$\mathcal{O}(k \cdot N \cdot D^2)$
	Relative-attention	$\mathcal{O}(N^2 \cdot D)$

Table 1. Per-layer complexity for different layer types.  $R$  is the resolution of voxels,  $v$  is number of voxel grids in a same box,  $N$  is the number of points,  $D$  is the representation dimension and  $k$  is the kernel size of convolutions.

robust. In this paper, we design our relative-attention to embed relative position representations which are not well studied in prior point cloud learning works.

First of all, by embedding RPR into the standard self-attention module, Eq 7 can be re-formulates as:

$$F_{ra} = \text{softmax}(QK^T + B)V \quad (9)$$

where  $B \in \mathbb{R}^{N \times N}$  is the relative representations bias.

Suppose that the original point cloud with  $N$  points is denoted by  $\mathcal{P} = \{p_i\}_{i=1}^N \subseteq \mathbb{R}^3$ , each point  $p_i = \{x_i, y_i, z_i\}$  and the relative position  $p_i - p_j$  is a 3D coordinate. We compute position difference on  $xyz$  directions separately, then summarizes them, which is given as follows:

$$B_{p_i, p_j} = (x_i - x_j) + (y_i - y_j) + (z_i - z_j). \quad (10)$$

This operation is highly efficient in the sense that it does not contain extra parameters and takes few FLOPs during inference. In addition, we hypothesized that precise relative position information is not useful beyond a certain distance. Clipping the maximum distance also enables the model to generalize to points' number not seen during training. Therefore, it can be described as:

$$B_{p_i, p_j} = \max(-\beta, \min(\beta, B_{p_i, p_j})), \quad (11)$$

where the scalar  $\beta$  is the maximum relative distance.

### 3.3. Feature Fusion

We effectively fuse the outputs of two branches with an addition as they are providing complementary information:

$$F' = F_{local} + F_{global}, \quad F' \in \mathbb{R}^{N \times D} \quad (12)$$

### 3.4. Relationship to prior works

The proposed PVT is related to several prior works which includes PVCNN [25], PCT [12], PT<sup>1</sup>[8], PT<sup>2</sup>[59].

Although we are inspired by the idea of PVCNN [25], our PVT is different: 1) in the *voxel* branch, PVCNN uses a 3D convolution to gather local information while we employ SWA computation within each local window, which is highly efficient (see Table 1,  $k \cdot D > v$ .  $v$  is 64 and  $D$  is

128 in our settings. In PVCNN's setting, the kernel size  $k$  is 3). 2) in the *point* branch, PVCNN uses a 1D convolution which is computation efficient but lacks the global context modeling capability. By performing RA computation on the entire points, our method gathers the global modeling power.

Unlike prior Transformer-based 3D models that need to gather the downsampled points and find the correspond neighbors by using expensive FPS and  $k$ -NN in *point* domain, our approach does not require explicitly identify which point is the farthest and what are in the neighboring set. Instead, the *voxel* branch observes regular data and learns to capture local features using SWA. Additionally, the *point* branch only needs to perform RA on the entire point cloud, which also does not require to find the neighboring points. Thus, our approach obtains highly efficient than PCT, PT<sup>1</sup> and PT<sup>2</sup> (see Table 3).

## 4. Experiments

We now discuss the PVT that can be constructed from PVT blocks for different point cloud learning tasks: shape classification, object and scene segmentation. The performance is quantitatively evaluated with four metrics, including overall accuracy (OA), average precision (AP) and the intersection over union (IoU), as well as mean IoU (mIoU). For the sake of fair comparison with baselines, we report the measured latency on a GTX 2080 GPU to reflect the efficiency but evaluate other indicators on a GTX 3090 GPU.

**Model.** The architecture used for the segmentation task is shown in Figure 1. In our settings, dropout with keep probability of 0.5 is used in the last two linear layers. All layers include ReLU and batch normalization. In addition, for other point cloud learning tasks, we use the similar architecture as in segmentation. Readers can refer to our source code for more details.

**Baselines.** We select four models as the comparison baselines, including the strong attention-based model PointASNL, and the three powerful Transformer-based networks PT<sup>1</sup>, PT<sup>2</sup> and PCT.

### 4.1. Shape Classification

**Data.** We conduct the classification experiment on the ModelNet40 [44] dataset. ModelNet40 includes 12,311 CAD models from 40 different object classes, in which 9843 models are used for training and the rest for testing. We follow the experimental configuration of PointNet, i.e., for each model, we uniformly sample 1024 points with 3 channels(or 6) of spatial location (and normal) as input; the point cloud is re-scaled to fit the unit sphere.

**Setting.** We utilized random translation, random anisotropic scaling and random input dropout strategies to augment the input points data during training. During testing, no data augmentation or voting methods were used. For

Model	Input	points	OA(%)	Latency
OA<92.5				
PointNet	xyz	16×1024	89.2	<b>13.6ms</b>
PointNet++ [29]	xyz,nor	16×1024	91.9	35.3ms
SO-Net [20]	xyz,nor	8×2048	90.9	—
PointGrid [19]	xyz,nor	16×1021	92.0	—
SpiderCNN [48]	xyz,nor	8×1024	92.4	82.6ms
PointCNN [21]	xyz	16×1024	92.2	221.2ms
PointWeb [58]	xyz,nor	16×1024	92.3	—
PVCNN [25]	xyz,nor	16×1024	92.4	24.2ms
OA>92.5				
KPCConv [36]	xyz	16×6500	92.9	120.5ms
DGCNN [42]	xyz	16×1024	92.9	85.8ms
LDGCNN [53]	xyz	16×1024	92.7	—
PointASNL [49]	xyz,nor	16×1024	93.2	923.6ms
PT <sup>1</sup> [8]	xyz,nor	16×1024	92.8	320.6ms
PT <sup>2</sup> [59]	xyz,nor	8×1024	93.7	530.2ms
PCT [12]	xyz	16×1024	93.2	92.4ms
PVT (Ours)	xyz	16×1024	93.6	<b>45.5ms</b>
PVT (Ours)	xyz,nor	16×1024	<b>94.0</b>	48.6ms

Table 2. Results on ModelNet40 [45]. Compared with previous Transformer-based models, our PVT achieves the state-of-the-art accuracy with 10× measured speed-up on average.

Model	Params	FLOPs	SDA(%)	OA(%)
PointNet	3.47M	0.45G	0.0	89.2
PointNet++(SSG)	1.48M	1.68G	43.5	90.7
PointNet++(MSG)	1.74M	4.09G	47.6	91.9
DGCNN	1.81M	2.43G	57.2	92.9
PointASNL	3.98M	5.92G	39.8	93.1
PT <sup>1</sup>	3.45M	3.48G	32.5	92.8
PT <sup>2</sup>	5.69M	5.90G	65.4	93.7
PCT	2.88M	2.17G	24.6	93.2
PVT(Ours)	<b>2.45M</b>	<b>1.62G</b>	<b>6.2</b>	<b>94.0</b>

Table 3. Computational resource requirements. SDA means the rate of total runtime on structuring the sparse data.

classification on ModelNet40, the SGD optimizer was used for 200 epochs with the batch size 32. We set the initial learning rate to 0.01 and adopt a cosine annealing schedule to adjust the learning rate at every epoch.

**Results.** The results are shown in Table 2, we can see that our PVT outperforms most previous models. Compared with its baselines, such as PCT, PT<sup>1</sup> and PT<sup>2</sup>, PointASNL, our PVT not only achieves state-of-the-art accuracy of 94.0%, but also has the best speed-accuracy trade-off (10× faster on average). In addition, Figure 3 provides an accuracy plot under equal-epoch setting. As can be seen, our method outperforms all Transformer-based methods, being the *fastest* and *most accurate* towards convergence.

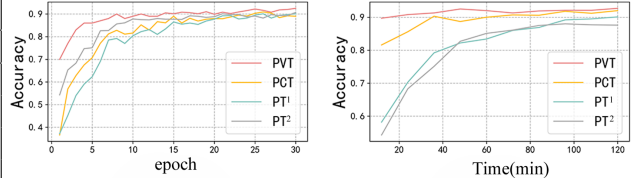


Figure 3. The accuracy of different Transformer-based methods over time and epochs on ModelNet40. In both equal-time and equal-epoch comparisons, our method performs the best. The accuracy of 90% can be achieved not only after 8 epochs but also in the shortest training time.

## 4.2. Computational requirements analysis

Now, we analysis the computational requirements of PVT and several other baselines by comparing the floating point operations required (FLOPs) and number of parameters (Params) in Table 3. PVT has the lowest memory requirements with only 2.45M parameters and also puts a low load on the processor of only 1.62G FLOPs, yet delivers highly accurate results of 94.0%. These characteristics make it suitable for deployment on a mobile device. In addition, PT 2 has attained top accuracy on various point cloud learning benchmarks, but its shortcomings of slow inference time and high computing cost are also obvious. And we summarize Table 3 the PVT only spend 6.3% of the total runtime on structuring the irregular data, which is much lower than previous Transformer-based models. In summary, PVT has best accuracy, the lowest computational and memory requirements compared with its baselines.

## 4.3. Object Part Segmentation

**Data.** The model is also evaluated on ShapeNet Parts [22]. It is composed of a total of 16,880 models (14,006 models are used for training, the rest for testing), each of those is has 2 to 6 parts and the whole dataset is labeled in 50 different parts. 2048 points are sampled from each model as input and only few point sets have six labeled parts. We directly adopt the same train-test split as PointNet in our experiment.

**Setting.** The same training setting as in our classification task was adopted. For this task on ShapeNet Part, we train our model using the SGD optimizer for 200 epochs with the batch size 16. The initial learning rate was set to 0.1, with a cosine annealing schedule to adjust the learning rate at every epoch.

**Results.** Table 4 lists the class-wise segmentation results. Part-average IoU is used to evaluate our model, which is given both overall and for each object category. The results show that our PVT makes an improvement of 2.9% over PointNet. Compared with all baselines, PVT attains the top pIoU with 86.6%.

**Visualization.** In Figure 4, we illustrate output fea-

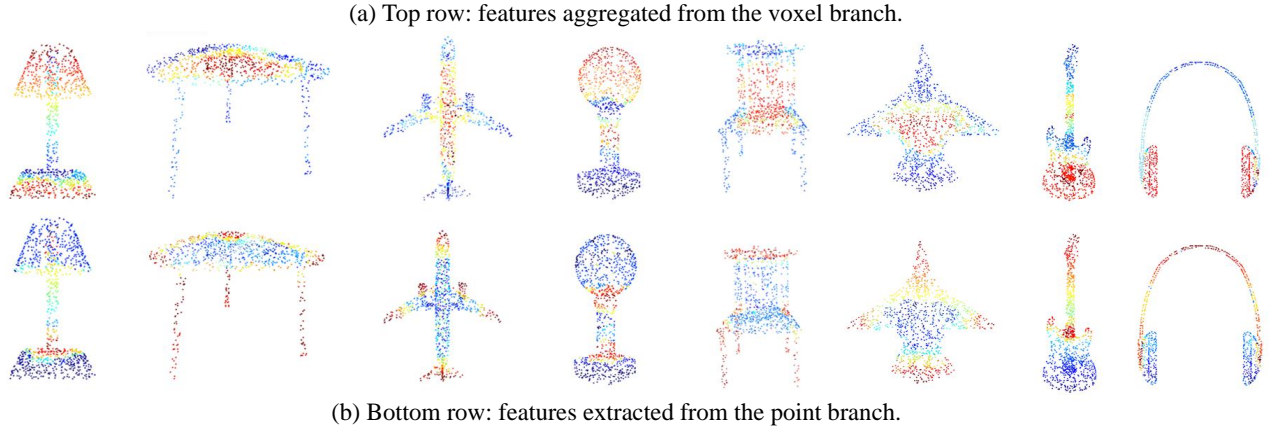


Figure 4. We demonstrate the output features extracted from two branches using Open3D [60]. The *voxel* branch focuses on the large, continuous parts, while the *point*-based captures the global shape details.

Model	pIoU	Areo	Bag	Cap	Car	Chair	Ear Phone	Guitar	Knife	Lamp	Laptop	Motor	Mug	Pistol	Rocket	Skate Board	Table
# Shapes		2690	76	55	898	3758	69	787	392	1547	451	202	184	283	66	152	5271
PointNet	83.7	83.4	78.7	82.5	74.9	89.6	73.0	91.5	85.9	80.8	95.3	65.2	93.0	81.2	57.9	72.8	80.6
P2Sequence	85.1	82.6	81.8	87.5	77.3	90.8	77.1	91.1	86.9	83.9	95.7	70.8	94.6	79.3	58.1	75.2	82.8
PointASNL	86.1	84.1	84.7	87.9	79.7	92.2	73.7	91.0	87.2	84.2	95.8	74.4	95.2	81.0	63.0	76.3	83.2
RS-CNN	86.2	83.5	<b>84.8</b>	88.8	79.6	91.2	<b>81.1</b>	<b>91.6</b>	88.4	86.0	<b>96.1</b>	73.7	94.1	83.4	60.5	<b>77.7</b>	<b>83.6</b>
PT <sup>1</sup>	85.9	—	—	—	—	—	—	—	—	—	—	—	—	—	—	—	—
PCT	86.4	85.0	82.4	<b>89.0</b>	81.2	91.9	71.5	91.3	88.1	<b>86.3</b>	95.8	64.6	<b>95.8</b>	83.6	62.2	77.6	73.7
PVT (Ours)	<b>86.6</b>	<b>85.3</b>	82.1	88.7	<b>82.1</b>	<b>92.4</b>	75.5	91.0	<b>88.9</b>	85.6	95.4	<b>76.2</b>	94.7	<b>84.2</b>	<b>65.0</b>	75.3	81.7

Table 4. Results of part segmentation on ShapeNet. pIoU means part-average Intersection-over-Union.

tures from the *point* and *voxel* branches respectively, where warmer color represents larger magnitude. As we can see, the *voxel* branch captures large, continuous parts while the *point*-based counterpart captures global shape details (e.g., table legs, airplane wings and tail).

#### 4.4. Indoor Scene Segmentation

**Data.** To further assess our network, we conduct semantic segmentation task on S3DIS dataset [1], which includes 273 million points from 6 indoor areas of 3 different buildings. Each point is annotated with a semantic label from 13 classes—e.g. beam, bookcase, chair, column, and window. We follow [35] and [27] and uniformly sampled points from blocks of area size  $1m \times 1m$ , where each point is represented by a 9-dimensional vector (XYZ, RGB, and normalized spatial coordinates).

**Setting.** During the training process, we generate training data by randomly sampling 4,096 points from each block on-the-fly. Following [42], we utilize Area-5 as the test scene and all the other areas for training. Note that the position and RGB information of points are used to as the input features. The same training setting as in our classi-

fication task was adopted, but requires 50 epochs with the batch size 8 to fulfil the experiment.

**Results.** The results are presented in Tables 5 and Table 6. From Tables 5, we can see that our PVT attains mIoU of 67.3%, which outperforms MLPs-based frameworks such as PointNet [27] and PointNet++ [29], graph-based methods such as DGCNN [42], attention-based models such as PointASNL [49]. Moreover, PVT attains mIoU of 69.2% under 6-fold cross-validation, substantially outperforming most prior models.

**Visualization.** Fig 5 shows the visualization of PVT’s predictions. The predictions of our network are very close to the ground truth. PVT captures detailed semantic structure in complex 3D scenes, which is important in our network.

#### 5. Ablation Studies

In this section, we conduct extensive ablation study to analyze the effectiveness of different components of PVT block. The results of the ablation study are summarized in Table 7 and 8.

##### Impact of the voxel-based and point-based branches.

Model	mIoU	Ceiling	Floor	Wall	Beam	Column	Window	Door	Chair	Table	Bookcase	Sofa	Board	Clutter
PointNet	41.09	88.80	97.33	69.80	0.05	3.92	46.26	10.76	52.61	58.93	40.28	5.85	26.38	33.22
PointNet++	50.04	90.79	96.45	74.12	0.02	5.77	43.59	25.39	69.22	76.94	21.45	55.61	49.34	41.88
PointNet++-CE	51.56	92.28	96.87	74.77	0.02	7.04	46.78	25.42	69.13	79.18	26.67	53.39	54.61	44.03
DGCNN	47.08	<b>92.42</b>	97.46	76.03	<b>0.37</b>	12.00	51.59	27.01	64.85	68.58	7.67	43.76	29.44	40.83
PVCNN	56.12	91.23	97.54	77.13	0.29	13.02	51.72	26.74	68.52	75.48	28.64	53.29	27.21	41.92
BPM [10]	61.43	—	—	—	—	—	—	—	—	—	—	—	—	—
PointASNL [10]	62.60	94.31	98.42	79.13	0.00	26.71	55.21	66.21	83.32	86.83	47.64	68.32	56.41	52.12
IAF-Net [46]	64.60	91.41	98.60	81.80	0.00	<b>34.90</b>	<b>62.00</b>	54.70	79.70	86.90	<b>49.90</b>	72.40	74.80	52.10
PVT(Ours)	<b>67.30</b>	91.18	<b>98.76</b>	<b>86.23</b>	0.31	34.21	49.90	<b>61.45</b>	<b>81.62</b>	<b>89.85</b>	48.20	<b>79.96</b>	<b>76.45</b>	<b>54.67</b>

Table 5. Indoor scene segmentation results on the S3DIS dataset, evaluated on Area5. From this table, we can see that the proposed PVT outperforms most of previous 3D models in some categories significantly,

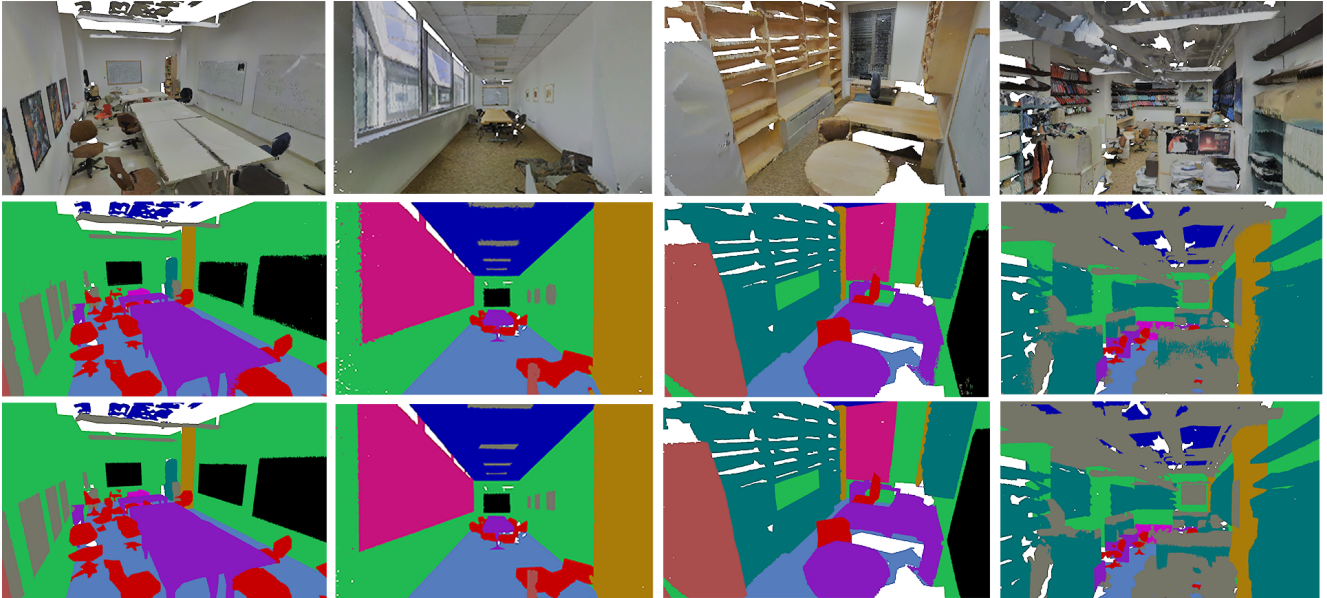


Figure 5. Visualization of semantic segmentation results on the S3DIS dataset. The input is in the top row, PVT predictions on the middle, the ground truth on the bottom.

Model	mIoU(%)	OA(%)	mAcc(%)
PointNet	47.6	78.5	66.2
G+RCU [9]	49.7	81.1	—
TangentConv [34]	52.8	—	—
RSNet [26]	56.5	—	66.5
3P-RNN [52]	56.3	86.9	—
SGPN [41]	50.4	—	—
SPGraph [18]	62.1	85.5	73.0
HAPGN [4]	62.9	85.8	—
PVCNN	63.2	85.8	72.5
ShellNet [55]	66.8	87.1	—
PVT(Ours)	<b>69.2</b>	<b>88.3</b>	<b>76.2</b>

Table 6. Results of semantic segmentation of 3D indoor scenes on S3DIS, evaluated with 6-fold cross-validation. From this table, we can see that the proposed PVT outperforms most of previous 3D models.

Model	PB	VB	shifting	NPB	OA(%)	Latency
A	✗	✓	✓	3	92.8	33.5
B	✓	✗	✓	3	92.3	25.2
C	✓	✓	✗	3	93.0	47.9
D	✓	✓	✓	2	93.1	36.4
E	✓	✓	✓	4	93.6	72.5
PVT <i>full</i>	✓	✓	✓	3	<b>94.0</b>	48.6

Table 7. Ablation study on ModelNet40. PB and VB mean the point-based branch and the voxel-based branch; NPB denotes the number of PVT blocks; shifting means all self-attention modules adopt the cyclic shifted box partitioning method.

We set two baselines: A and B. Model A only encodes global context features by the *point* branch, and Model B only encodes local features by the *voxel* one. As reported in Table 7, the Baseline model A obtains a low accu-

Ablation	ModelNet40(OA)	ShapeNet(mIoU)
MLP	92.6	85.3
EdgeConv	93.1	85.8
w/o rel. pos	93.2	86.3
PVT <sup>full</sup>	<b>94.0</b>	<b>86.6</b>

Table 8. Ablation study on the relative-attention and relative position bias on two benchmarks. MLP: replace relative-attention with MLP layer in our architecture. EdgeConv: replace relative-attention with EdgeConv layer in our architecture. no rel. pos: the relative attention without an additional relative position bias term (see Eq 9).

racy of 92.8% on classification benchmarks, and model B gets 92.3%. When we combine local and global features (PVT<sup>full</sup>), there is a notable improvement in both tasks. This means our network can take advantage of the combination of two branches, which provides richer information about the points.

**Effect of the cyclic shifted windows scheme.** Ablation of the *shifted window* method on classification are reported in Table 7 (Model C). The network with the *shifted window* partitioning (PVT<sup>full</sup>) outperforms the Model C without shifting at each layer by +1.0% OA on ModelNet40. The results indicate the effectiveness and efficiency of using cyclic shifted window to build cross-window information interaction in the preceding layers.

**Impact of the number of PVT blocks.** we validate the impact of the PVT block by controlling the number of PVT blocks and report the results in Table 7. From this table we can conclude the following: on one hand, reducing the number of PVT block can save latency, for example, compare with PVT<sup>full</sup>, Model D saves 25% latency but incurs a loss on accuracy; on the other hand, increasing the number of PVT block from PVT<sup>full</sup> can hardly support Model E accuracy benefit but leads to an increase on latency. To balance between speed and accuracy, we adopt 3 PVT blocks as our full model.

**Effect of Relative-attention.** We validate the impact of RA module used in our network. The results are shown in Table 8. We set two baselines. ‘MLP’ is a no-attention baseline that we replaces RA with a MLP layer. ‘EdgeConv’ is a more advanced no-attention baseline that we replaces RA with a EdgeConv layer. EdgeConv performs feature aggregating at each point and enables each point to exchange information with its neighboring points, but does not leverage attention mechanisms. We can see that the RA module achieves better results than the no-attention baselines. The performance gap between RA and MLP baselines is significant: 94.0% vs. 92.6% and 86.6% vs. 85.3%, an improvement of 1.4 and 1.3 absolute percentage points. Compare with EdgeConv baseline, our RA module also achieves improvements of 0.9 and 0.9 absolute percentage points.

**Effect of relative position representations.** Finally, we also investigate the impact of RPR used in the RA module. As demonstrated in Table 8, we can see that our PVT with RPR yields +0.8% OA/+0.4% mIoU on ModelNet40 and ShapeNet in relation to those without this term respectively, indicating the effectiveness of the RPR.

## 6. Conclusion and Future Work

In this work, we present Point-Voxel Transformer for efficient point cloud learning, that is found to surpass previous Transformer-based and attention-based models in efficiency. It achieves this by deeply combining the advantages from both the *voxel*-based and the *point*-based networks. To reduce the computation cost, we design a GPU-based SWA computing method which has linear computational complexity with respect to voxel resolution. In addition, we present RA module, a relation-aware self-attention for modeling relative position representations, to improve the recognition accuracy for point cloud learning tasks.

In the future, we expect to promote the primary structure for other research areas, such as point cloud generation and completion.

## Acknowledgments

This work was partially supported by the Zhejiang Provincial Natural Science Foundation of China (LGF21F20012), the National Natural Science Foundation of China (No.61602139), and the Graduate Scientific Research Foundation of Hangzhou Dianzi University (CXJJ2021082, CXJJ2021083).

## References

- [1] I. Armeni, S. Sax, A. R. Zamir, and S. Savarese. Joint 2d-3d-semantic data for indoor scene understanding. *arXiv preprint arXiv:1702.01105*, 2017. 2, 7
- [2] Bahdanau, Dzmitry, K. Cho, and Y. Bengio. Neural machine translation by jointly learning to align and translate. *in ICLR*, 2014. 3
- [3] C. Chen, G. Li, R. Xu, T. Chen, M. Wang, and L. Lin. Clusternet: Deep hierarchical cluster network with rigorously rotation-invariant representation for point cloud analysis. *Proceedings of the IEEE/CVF Conference on Computer Vision and Pattern Recognition*, 2020. 1
- [4] C. Chen, S. Qian, Q. Fang, and C. Xu. Hapgn: Hierarchical attentive pooling graph network for point cloud segmentation. *IEEE Transactions on Multimedia*, 23:2335–2346, 2021. 8
- [5] C. Choy, J. Y. Gwak, and S. Savarese. 4d spatio-temporal convnets: Minkowski convolutional neural networks. *Proceedings of the IEEE/CVF Conference on Computer Vision and Pattern Recognition*, 2019. 2
- [6] J. Devlin, M. W. Chang, K. Lee, and K. Toutanova. Bert: Pre-training of deep bidirectional transformers for language understanding. *in NAACL-HLT*, 2018. 3

- [7] A. Dosovitskiy, L. Beyer, A. Kolesnikov, D. Weissenborn, X. Zhai, T. Unterthiner, M. Dehghani, M. Minderer, G. Heigold, S. Gelly, J. Uszkoreit, and N. Houlsby. An image is worth 16x16 words: Transformers for image recognition at scale. *in ICLR*, 2021. 1, 3
- [8] N. Engel, V. Belagiannis, and K. Dietmayer. Point transformer. *CoRR*, abs/2011.00931, 2020. 1, 2, 3, 5, 6
- [9] F. Engelmann, T. Kontogianni, A. Hermans, and B. Leibe. Exploring spatial context for 3d semantic segmentation of point clouds. *2017 IEEE International Conference on Computer Vision Workshop (ICCVW)*, 2017. 8
- [10] J. Gong, J. Xu, X. Tan, J. Zhou, Y. Qu, Y. Xie, and L. Ma. Boundary-aware geometric encoding for semantic segmentation of point clouds. *Proceedings of the AAAI Conference on Artificial Intelligence*, 2021. 8
- [11] B. Graham, M. Engelcke, and L. van der Maaten. 3d semantic segmentation with submanifold sparse convolutional networks. In *2018 IEEE Conference on Computer Vision and Pattern Recognition, Salt Lake City, UT, USA, June 18-22*, pages 9224–9232. Computer Vision Foundation / IEEE Computer Society, 2018. 4
- [12] M.-H. Guo, J.-X. Cai, Z.-N. Liu, T.-J. Mu, R. R. Martin, and S.-M. Hu. Pct: Point cloud transformer. *Computational Visual Media*, 7(2):187–199, Apr 2021. 1, 2, 3, 5, 6
- [13] H. Hu, Z. Zhang, Z. Xie, and S. Lin. Local relation networks for image recognition. *IEEE/CVF International Conference on Computer Vision (ICCV)*, 2019. 3
- [14] Q. Huang, W. Wang, and U. a. Neumann. Recurrent slice networks for 3d segmentation of point clouds. *Proceedings of the IEEE/CVF Conference on Computer Vision and Pattern Recognition*, 2018. 2
- [15] R. Klokov and V. Lempitsky. Escape from cells: Deep kd-networks for the recognition of 3d point cloud models. *Proceedings of the IEEE International Conference on Computer Vision*, pages 863–872, 2017. 2
- [16] S. Lan, R. Yu, G. Yu, and L. S. Davis. Modeling local geometric structure of 3d point clouds using geo-cnn. *Proceedings of the IEEE/CVF Conference on Computer Vision and Pattern Recognition*, 2019. 1
- [17] L. Landrieu and M. Boussaha. Point cloud oversegmentation with graph-structured deep metric learning. *Proceedings of the IEEE/CVF Conference on Computer Vision and Pattern Recognition*, 2020. 3
- [18] L. Landrieu and M. Simonovsky. Large-scale point cloud semantic segmentation with superpoint graphs. *IEEE Conference on Computer Vision and Pattern Recognition (CVPR)*, 2018. 8
- [19] T. Le and D. Ye. Pointgrid: A deep network for 3d shape understanding. *Proceedings of the IEEE/CVF Conference on Computer Vision and Pattern Recognition*, 2018. 2, 6
- [20] J. Li, B. M. Chen, and G. H. Lee. So-net: Self-organizing network for point cloud analysis. *Proceedings of the IEEE/CVF Conference on Computer Vision and Pattern Recognition*, 2018. 6
- [21] Y. Li, R. Bu, M. Sun, and B. Chen. Pointcnn: Convolution on x-transformed points. *Advances in Neural Information Processing Systems (NeurIPS)*, 2018. 6
- [22] Y. Li, V. G. Kim, D. Ceylan, I. C. Shen, M. Yan, S. Hao, C. Lu, Q. Huang, A. Sheffer, and L. Guibas. A scalable active framework for region annotation in 3d shape collections. *ACM Transactions on Graphics (TOG)*, 35(6cd):210.1–210.12, 2016. 2, 6
- [23] Z. Lin, M. Feng, C. N. d. Santos, M. Yu, B. Xiang, B. Zhou, and Y. Bengio. A structured self-attentive sentence embedding. *in ICLR*, 2017. 3
- [24] Z. Liu, Y. Lin, Y. Cao, H. Hu, Y. Wei, Z. Zhang, S. Lin, and B. Guo. Swin transformer: Hierarchical vision transformer using shifted windows. *IEEE/CVF International Conference on Computer Vision (ICCV)*, 2021. 1, 2, 3, 4
- [25] Z. Liu, H. Tang, Y. Lin, and S. Han. Point-voxel cnn for efficient 3d deep learning. *Advances in Neural Information Processing Systems (NeurIPS)*, 2019. 1, 2, 4, 5, 6
- [26] R. Mehta and T. Arbel. Rs-net: Regression-segmentation 3d cnn for synthesis of full resolution missing brain mri in the presence of tumours. *International Workshop on Simulation and Synthesis in Medical Imaging*, pages 119–129, 2018. 8
- [27] C. R. Qi, H. Su, K. Mo, and L. J. Guibas. Pointnet: Deep learning on point sets for 3d classification and segmentation. *Proceedings of the IEEE/CVF Conference on Computer Vision and Pattern Recognition*, pages 652–660, 2017. 2, 7
- [28] C. R. Qi, H. Su, M. Niebner, A. Dai, M. Yan, and L. J. Guibas. Volumetric and multi-view cnns for object classification on 3d data. *Proceedings of the IEEE/CVF Conference on Computer Vision and Pattern Recognition*, 2016. 1
- [29] C. R. Qi, L. Yi, H. Su, and L. J. Guibas. Pointnet++: Deep hierarchical feature learning on point sets in a metric space. *Advances in Neural Information Processing Systems (NeurIPS)*, 2017. 6, 7
- [30] P. Ramachandran, N. Parmar, A. Vaswani, I. Bello, A. Levskaya, and J. Shlens. Stand-alone self-attention in vision models. *CoRR*, abs/1906.05909, 2019. 3
- [31] G. Riegler, A. O. Ulusoy, and A. Geiger. Octnet: Learning deep 3d representations at high resolutions. *IEEE Computer Society*, 2016. 2
- [32] Q. Shi, S. Anwar, and N. Barnes. Semantic segmentation for real point cloud scenes via bilateral augmentation and adaptive fusion. *Proceedings of the IEEE/CVF Conference on Computer Vision and Pattern Recognition*, 2021. 2
- [33] S. Shi, C. Guo, L. Jiang, Z. Wang, J. Shi, X. Wang, and H. Li. Pv-rcnn: Point-voxel feature set abstraction for 3d object detection. *Proceedings of the IEEE/CVF Conference on Computer Vision and Pattern Recognition*, 2019. 1
- [34] M. Tatarchenko, J. Park, V. Koltun, and Q. Y. Zhou. Tangent convolutions for dense prediction in 3d. *Proceedings of the IEEE/CVF Conference on Computer Vision and Pattern Recognition*, 2018. 8
- [35] L. Tchapmi, C. Choy, I. Armeni, J. Y. Gwak, and S. Savarese. Segcloud: Semantic segmentation of 3d point clouds. *2017 International Conference on 3D Vision (3DV)*, 2017. 7
- [36] H. Thomas, C. R. Qi, J. E. Deschard, B. Marcotequi, and L. J. Guibas. Kpconv: Flexible and deformable convolution for point clouds. *IEEE/CVF International Conference on Computer Vision (ICCV)*, 2019. 6

- [37] A. Vaswani, N. Shazeer, N. Parmar, J. Uszkoreit, L. Jones, A. N. Gomez, L. Kaiser, and I. Polosukhin. Attention is all you need. *Advances in Neural Information Processing Systems (NeurIPS)*, 2017. 1, 3, 4
- [38] C. Wang, B. Samari, and K. Siddiqi. Local spectral graph convolution for point set feature learning. in *ECCV*, 2018. 1
- [39] L. Wang, Y. Huang, Y. Hou, S. Zhang, and J. Shan. Graph attention convolution for point cloud semantic segmentation. *Proceedings of the IEEE/CVF Conference on Computer Vision and Pattern Recognition*, 2019. 2
- [40] P. S. Wang, Y. Liu, Y. X. Guo, C. Y. Sun, and X. Tong. O-cnn: Octree-based convolutional neural networks for 3d shape analysis. *Acm Transactions on Graphics*, 36(4):72, 2017. 2
- [41] W. Wang, R. Yu, Q. Huang, and U. Neumann. Sgpn: Similarity group proposal network for 3d point cloud instance segmentation. *Proceedings of the IEEE Conference on Computer Vision and Pattern Recognition*, pages 2569–2578, 2018. 8
- [42] Y. Wang, Y. Sun, Z. Liu, S. E. Sarma, M. M. Bronstein, and J. M. Solomon. Dynamic graph cnn for learning on point clouds. *ACM Transactions on Graphics*, 38(5), 2018. 2, 6, 7
- [43] Z. Wang and F. Lu. Voxsegnet: Volumetric cnns for semantic part segmentation of 3d shapes. *IEEE Transactions on Visualization and Computer Graphics*, pages 1–1, 2019. 1
- [44] Z. Wu, S. Song, A. Khosla, X. Tang, and J. Xiao. 3d shapenets for 2.5d object recognition and next-best-view prediction. *Proceedings of the IEEE/CVF Conference on Computer Vision and Pattern Recognition*, 2014. 2, 5
- [45] Z. Wu, S. Song, A. Khosla, F. Yu, L. Zhang, X. Tang, and J. Xiao. 3d shapenets: A deep representation for volumetric shapes. *2015 IEEE Conference on Computer Vision and Pattern Recognition (CVPR)*, 2015. 6
- [46] M. Xu, Z. Zhou, J. Zhang, and Y. Qiao. Investigate indistinguishable points in semantic segmentation of 3d point cloud. *Proceedings of the AAAI Conference on Artificial Intelligence*, abs/2103.10339, 2021. 8
- [47] Q. Xu, X. Sun, C.-Y. Wu, P. Wang, and U. Neumann. Gridcnn for fast and scalable point cloud learning. *Proceedings of the IEEE/CVF Conference on Computer Vision and Pattern Recognition*, pages 5661–5670, 2020. 2
- [48] Y. Xu, T. Fan, M. Xu, Z. Long, and Q. Yu. Spidercnn: Deep learning on point sets with parameterized convolutional filters. *ECCV*, 2018. 6
- [49] X. Yan, C. Zheng, Z. Li, S. Wang, and S. Cui. Pointasnl: Robust point clouds processing using nonlocal neural networks with adaptive sampling. *Proceedings of the IEEE/CVF Conference on Computer Vision and Pattern Recognition*, 2020. 1, 6, 7
- [50] Y. Yan, Y. Mao, and B. Li. Second: Sparsely embedded convolutional detection. *Sensors*, 18(10), 2018. 2, 4
- [51] B. Yang, J. Wang, R. Clark, Q. Hu, S. Wang, A. Markham, and N. Trigoni. Learning object bounding boxes for 3d instance segmentation on point clouds. *Proceedings of the IEEE/CVF Conference on Computer Vision and Pattern Recognition*, 2019. 2
- [52] X. Ye, J. Li, H. Huang, L. Du, and X. Zhang. 3d recurrent neural networks with context fusion for point cloud semantic segmentation. *Proceedings of the European Conference on Computer Vision (ECCV)*, pages 403–417, 2018. 8
- [53] K. Zhang, M. Hao, J. Wang, C. D. Silva, and C. Fu. Linked dynamic graph cnn: Learning on point cloud via linking hierarchical features. *arXiv:1904.10014 [cs]*, 2019. 2, 6
- [54] W. Zhang and C. Xiao. Pcan: 3d attention map learning using contextual information for point cloud based retrieval. *Proceedings of the IEEE/CVF Conference on Computer Vision and Pattern Recognition*, 2019. 2
- [55] Z. Zhang, B. S. Hua, and S. K. Yeung. Shellnet: Efficient point cloud convolutional neural networks using concentric shells statistics. *2019 IEEE/CVF International Conference on Computer Vision (ICCV)*, 2019. 8
- [56] H. Zhao, J. Jia, and V. K. and. Exploring self-attention for image recognition. *Conference on Computer Vision and Pattern Recognition (CVPR)*, 2020. 3
- [57] H. Zhao, L. Jiang, C. W. Fu, and J. Jia. Pointweb: Enhancing local neighborhood features for point cloud processing. *Proceedings of the IEEE/CVF Conference on Computer Vision and Pattern Recognition*, 2019. 2
- [58] H. Zhao, L. Jiang, C.-W. Fu, and J. Jia. Pointweb: Enhancing local neighborhood features for point cloud processing. *Proceedings of the IEEE/CVF Conference on Computer Vision and Pattern Recognition*, pages 5565–5573, 2019. 6
- [59] H. Zhao, L. Jiang, J. Jia, P. Torr, and V. Koltun. Point transformer. *IEEE/CVF International Conference on Computer Vision (ICCV)*, 2021. 1, 2, 3, 5, 6
- [60] Q.-Y. Zhou, J. Park, and V. Koltun. Open3D: A modern library for 3D data processing. *arXiv:1801.09847*, 2018. 7
- [61] Y. Zhou and O. Tuzel. Voxelnet: End-to-end learning for point cloud based 3d object detection. *IEEE/CVF International Conference on Computer Vision (ICCV)*, pages 4490–4499, 2018. 1